Appl. Phys. B 79, 211–219 (2004)
DOI: 10.1007/s00340-004-1524-4

Applied Physics B
Lasers and Optics

S. SPIEKERMANN[1,✉]
F. LAURELL[1]
V. PASISKEVICIUS[1]
H. KARLSSON[2]
I. FREITAG[3]

Optimizing non-resonant frequency conversion in periodically poled media

[1] Department of Physics, Royal Institute of Technology, Roslagstullsbacken 21, 106 91 Stockholm, Sweden
[2] Cobolt AB, Kräftriket 8, 104 05 Stockholm, Sweden
[3] InnoLight GmbH, Garbsener Landstrasse 10, 30419 Hannover, Germany

Received: 5 January 2004/Revised version: 19 March 2004
Published online: 19 May 2004 •

ABSTRACT Non-resonant frequency conversion into the blue, green, orange, and red spectral regions is reported. Fundamental light sources were continuous-wave non-planar monolithic single-mode ring Nd : YAG lasers as well as a standing-wave multi-mode Nd : YAG laser. Periodically poled $KTiOPO_4$ was employed as the nonlinear medium, but the considerations could also be applied to other periodically poled materials. A multi-pass scheme resulted in a normalized conversion efficiency as high as 27.2 % W^{-1} for frequency doubling in the small-signal regime at 1064 nm.

PACS 42.65.Ky; 42.79.Nv; 42.70.Mp

1 Introduction

For many years birefringent phase matching with angle tuning was used for nonlinear frequency conversion. However, this technique only allows utilizing a limited number of nonlinear coefficients. For example, the large values of d_{33} in $LiNbO_3$ and $KTiOPO_4$ are not available with birefringent phase matching. As a consequence, high intensities were needed to achieve efficient frequency conversion. This was achieved by pulsing the laser, coupling single-frequency radiation into an external cavity, or placing the nonlinear crystal directly into the laser cavity. All these techniques have their drawbacks: only a limited number of applications are addressed with pulsed lasers. Employing an external cavity requires complicated electronics and the intra-cavity approach suffers in most cases from stability problems.

By the recent introduction of quasi-phase matching (QPM) in bulk frequency conversion, some of these difficulties have been reduced. By use of non-critical phase matching, walk-off can be avoided and hence longer crystals used without beam-quality degradation. Furthermore, a wider transparency range can be used, as the full transmission range is available by choosing the appropriate QPM grating. And, finally, the crystal axis with the highest nonlinear coefficient can be phase matched, leading to drastically enhanced conversion efficiency in many cases. Today two groups of crystals have successfully been periodically poled (PP) and employed for bulk QPM frequency conversion, those from the $LiNbO_3$ family ($LiNbO_3$, $LiTaO_3$, and $KNbO_3$ [1–3]) and those from the $KTiOPO_4$ (KTP) family ($KTiOPO_4$, $RbTiOAsO_4$, and $RbTiOPO_4$ [4–7]).

The first high conversion efficiency second-harmonic generation (SHG) experiments with PP crystals were done in $LiNbO_3$ by Miller et al. [8]. Compared to angle phase-matched $LiNbO_3$, the normalized conversion efficiency increased by one order of magnitude to 1.7 % W^{-1} cm^{-1} using a 53-mm-long sample and a fundamental power of 6.5 W. Later on, KTP was successfully poled and used for SHG [9]. Its normalized conversion efficiency is slightly lower than for $LiNbO_3$ (1.1 % W^{-1} cm^{-1} in single pass, 2.8 % W^{-1} cm^{-1} in double pass [10]), but it is rather insensitive to photorefractive damage, even when used at room temperature, which makes it particularly useful for experiments in the visible spectral range. Periodically poled crystals have also been used in waveguide configurations [11] and then the conversion efficiency is high even at moderate pump powers. This is due to the confinement effect of the waveguide. However, the output power has been limited to approximately 100 mW in these cases due to various types of damage.

In this letter, we provide a method for optimizing frequency conversion with PP materials in general, and with periodically poled KTP (PPKTP) in particular. We first introduce the theoretical background of quasi-phase matching and its potential to obtain a high SHG efficiency for a single-pass and then a multi-pass geometry. It follows the framework given by Fejer et al. [12]. Then we discuss some limitations that appear in practice. To some extent this was done already in [13], but only for the single-pass configuration. The calculations lead to a strategy, which was applied for the experiments. There we tried to consider and investigate all the possible limitations. Altogether this resulted in an experimental SHG conversion efficiency as high as 27.2 % W^{-1}. To the best of our knowledge, this represents the highest value ever achieved for a non-resonant frequency-converting scheme in a bulk nonlinear medium.

2 Introduction to QPM

Efficient energy transfer in nonlinear frequency-conversion processes requires phase matching, i.e. main-

✉ Fax: +46-8/55-378-216, E-mail: sp@laserphysics.kth.se

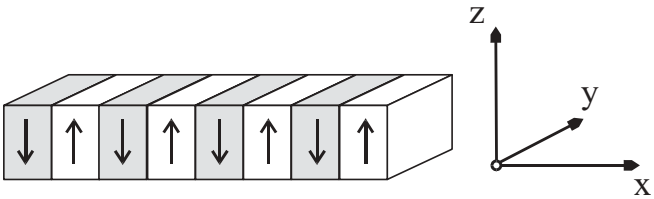

FIGURE 1 Geometry of the periodic polarization reversal in PPKTP

tenance of a constant phase relation between the interacting waves during their propagation through the nonlinear medium. This can be obtained by QPM, where an artificially engineered spatial modulation of the nonlinear coefficient (periodic polarization reversal, see Fig. 1) is used to periodically reset the accumulated phase error between the driving and the generated waves [14]. The wave-vector mismatch for the mth-order QPM second harmonic generation (SHG) collinear process is expressed as

$$\Delta \boldsymbol{k}_Q = \boldsymbol{k}_{2\omega} - 2\boldsymbol{k}_\omega - \boldsymbol{k}_G, \tag{1}$$

with the grating vector

$$|\boldsymbol{k}_G| = m\frac{2\pi}{\Lambda}, \tag{2}$$

where the period Λ is twice the coherence length for the interacting waves. Manufacturing a period of 9 μm for first-order ($m = 1$) SHG at 1064 nm is state of the art for KTP. For shorter wavelengths, dispersion increases rapidly and the coherence lengths become on the order of a few μm. Periods as short as 2.95 μm have already been realized in KTP for SHG at 780 nm [15], but the fabrication is still rather difficult over large areas.

Let us, for the sake of simplicity, assume that the fabricated structure is ideal (the influence of imperfections is treated in [12, 16]) and has an optimum duty cycle for the polarization reversal. The effective nonlinear coefficient d_{eff} is then reduced by the Fourier amplitude of the mth spatial harmonic of the mth spatial harmonic of the rectangular modulation of the relevant nonlinear coefficient d_{ij}.

$$d_{\text{eff}} = \frac{2}{m\pi} d_{ij}. \tag{3}$$

In our experiments, we used light polarized along the z axis of KTP, which corresponds to use of $d_{ij} = d_{33} = 16.9$ pm/V. The equation for SHG with a Gaussian beam profile is [17]

$$P_{\text{SHG}} = Kl\boldsymbol{k}_\omega P_{\text{F}}^2 h\mathrm{e}^{-\alpha l}, \tag{4}$$

with the coupling constant

$$K = \frac{2\omega^2 d_{\text{eff}}^2}{\pi n_{2\omega} n_\omega^2 \varepsilon_0 c^3}, \tag{5}$$

the focusing-dependent numerical value h (Boyd–Kleinman factor), the absorption coefficient α, and the crystal length l. The conversion efficiency in the high-conversion regime, i.e. when we have pump depletion, is

$$\eta(P_{\text{F}}) = \tanh^2\left[\left(Kl\boldsymbol{k}_\omega P_{\text{F}} h\mathrm{e}^{-\alpha l}\right)^{1/2}\right]. \tag{6}$$

It is proportional to d_{eff}^2, although reduced by the factor $(2/m\pi)^2$, still several times larger than for a conventional birefringent phase-matched interaction. In a first-order QPM SHG interaction in KTP it is on the order of 10 due to the high d_{33} coefficient utilized, which is not accessible in angle-tuned birefringent phase matching. Depending on the interacting wavelengths and the quality of the grating structure, d_{eff} can reach values up to 11 pm/V (with birefringent phase matching up to 3.3 pm/V). With confocal focusing, h is maximized, and the normalized conversion efficiency for SHG reaches more than 1.1 % $\text{W}^{-1}\,\text{cm}^{-1}$ with diffraction-limited single-frequency radiation at 1064 nm. In the plane-wave case the second-harmonic (SH) field grows quadratically with the crystal length, but for a focused Gaussian beam it grows only linearly with the crystal length. This can be overcome by reflecting the beam and then refocusing it N times through the crystal. The efficiency then scales with $N^2 l$ (Imeshev et al. reported an enhancement with a factor of 3.7 for refocusing a second time [21]). Therefore, this is a very appealing technique for frequency conversion of broadband fundamental pump sources, since the bandwidth decreases with only Nl.

3 Limitations for harmonic generation

3.1 *Acceptance bandwidths*

Even under optimized focusing conditions and using diffraction-limited beams, the SHG conversion efficiency can be reduced by means of wavelength, temperature, and angular acceptance bandwidth limitations. In other words, the conversion efficiency will be affected if the line width of the fundamental laser source is in the range of or larger than the wavelength acceptance bandwidth of the QPM crystal [16]. For a perfectly uniform grating, the wavelength acceptance bandwidth is given by [12]

$$\Delta\lambda_{\text{FWHM}} = \frac{0.4429\lambda_{\text{F}}}{l}\left[\frac{n_{\text{SH}} - n_{\text{F}}}{\lambda_{\text{F}}} + \frac{\partial n_{\text{F}}}{\partial \lambda_{\text{F}}} - \frac{1}{2}\frac{\partial n_{\text{SH}}}{\partial \lambda_{\text{SH}}}\right]^{-1}. \tag{7}$$

The SHG wavelength-tuning bandwidth for a 1-cm-long PPKTP sample in confocal focusing is plotted in Fig. 2. Here we

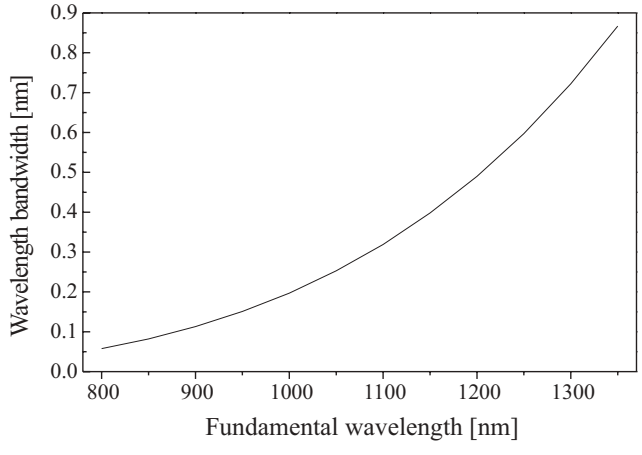

FIGURE 2 Calculated wavelength acceptance bandwidth as a function of the fundamental wavelength for type-I QPM SHG in a 1-cm-long PPKTP crystal

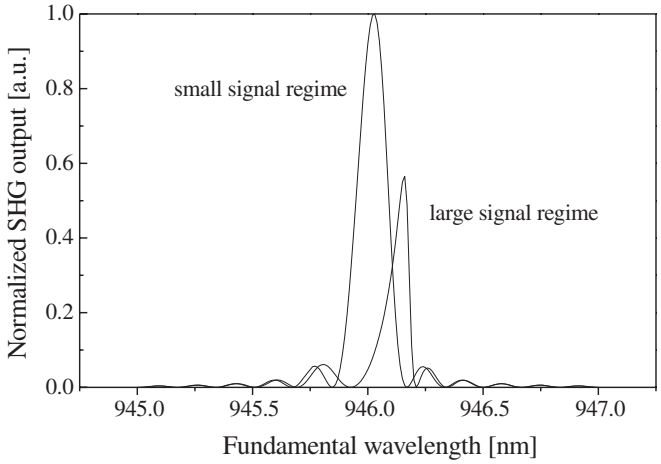

FIGURE 3 Simulated wavelength-tuning curves for SHG in a 0.5-cm-long PPKTP crystal ($\Lambda = 6.09\,\mu$m). The small-signal regime is shown as well as the large-signal regime where SH absorption induces substantial temperature fluctuations in the sample

used [19] to calculate the derivatives of the refractive indices with wavelength. The sinc-tuning curve for SHG with a fundamental wavelength of 946 nm ($\Lambda = 6.09\,\mu$m) is shown in Fig. 3. In this figure we also demonstrate the effect of non-uniform crystal heating due to SH absorption. We assume a heating process giving rise to a temperature increase proportional to the square of the SH amplitude. To fit with the experiments we chose it to be 2 W at the end of the crystal. We refer to [20] as a tool for calculating these temperature gradients. It is clearly seen that in the large-signal regime the relative conversion efficiency decreases and the acceptance bandwidth narrows. We will give experimental proof of this effect in Sect. 4.5.

Besides $\Delta\lambda$, the temperature acceptance bandwidth is another important variable in our experiments. It has to be large enough to overcome the effect raised by temperature gradients in the crystal and it determines the requirements for the stability of the temperature controller. With a fixed wavelength, it can be expressed as [12]

$$\Delta T_{\mathrm{FWHM}} = \frac{0.4429\lambda_{\mathrm{F}}}{l} \times \left[\left.\frac{\partial n_{\mathrm{SH}}}{\partial T}\right|_{T_0} - \left.\frac{\partial n_{\mathrm{F}}}{\partial T}\right|_{T_0} + \alpha(n_{\mathrm{SH}} - n_{\mathrm{F}}) \right]^{-1}. \quad (8)$$

The angular acceptance bandwidth, $\Delta\varphi$, is important when focusing with large numerical aperture or when employing a double-pass scheme where the angle formed between the forward- and backward-propagating beams is non-zero. When the PPKTP sample is rotated around the z axis away from ideal non-critical phase matching, Fejer et al. [12] determined:

$$\Delta\varphi = 2\sqrt{1.772\frac{n_{\mathrm{SHG}}}{n_{\mathrm{F}}}\frac{\Lambda}{2l}\cos\varphi}. \quad (9)$$

Here φ is defined as the angle between the wave vector for the incident fundamental beam and the pseudo-momentum vector associated with the periodic lamellar domains.

$\Delta\lambda$	ΔT	$\Delta\varphi$
0.27 nm/cm	5.94 K/cm	3.26 °/cm$^{1/2}$

TABLE 1 Acceptance bandwidths as a function of crystal length l at a fundamental wavelength of 1064 nm

In Table 1 we have calculated the three different SHG acceptance bandwidths as a function of crystal length for PPKTP utilizing d_{33} interaction and a fundamental wavelength of 1064 nm.

3.2 *Linear phase-front distortion*

Despite the problems, which arise from bandwidth limitations, there is one effect that exclusively occurs when QPM materials are applied in multiple-pass schemes. Imeshev et al. first pointed out that the phase front of the harmonic beam that propagates across the output boundary of the crystal would be subjected to a linear distortion arising from an angle θ, formed by the grating and the output boundary [21]. This results, under certain conditions, in destructive interference effects when the beam is reflected back for a second frequency-converting step (see Fig. 4). Moreover, the beam quality and the conversion efficiency will decrease, depending on the beam radius and the angle θ. In [21], this problem is treated in detail. Extensive simulations using both three-dimensional and plane-wave calculations were performed in [22]. Here, we just want to give the equation that approximates the wedge angle $\theta_{95\%}$, where the SH power is reduced by $\approx 5\%$:

$$\theta_{95\%} \approx \frac{0.2\Lambda}{2\omega_{\mathrm{b}}}, \quad (10)$$

with the fundamental beam radius ω_{b} (at $1/\mathrm{e}^2$ of the intensity) at the crystal boundary that causes the phase-front distortion. For small distortions, one can estimate that the beam quality degrades by the same amount as the SH power [21]. Therefore, the M^2 value is 1.05 for the 95% case. However, in Sect. 4.5 it will turn out that (10) is not accurate enough. We solved this problem numerically by assuming that the double-pass conversion efficiency changes sinusoidally when translating an infinitely small back-reflected beam over the crystal boundary in the y direction [21]. The total normalized conversion efficiency, η_{tot}, of the beam is then just the integral over its Gaussian profile, multiplied with the phase-shift-induced modulation. As a result, one can then obtain η_{tot} not only for

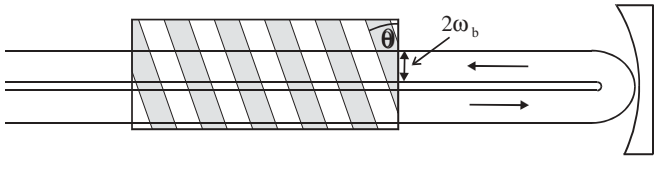

FIGURE 4 Schematic sketch of a double pass through a periodically poled medium. θ is the angle formed by the grating structure and the crystal boundary, while the beam radius at this boundary is ω_{b}

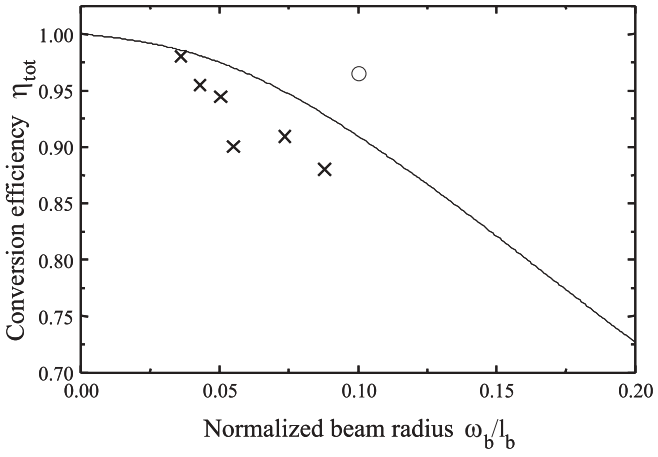

FIGURE 5 The reduction of the conversion efficiency to η_{tot}, when employing a normalized beam radius ω_b/l_b to a wedged PPKTP. The *crosses* show the experimental data. The *circle* is calculated from (10) and the *curve* is obtained from (11)

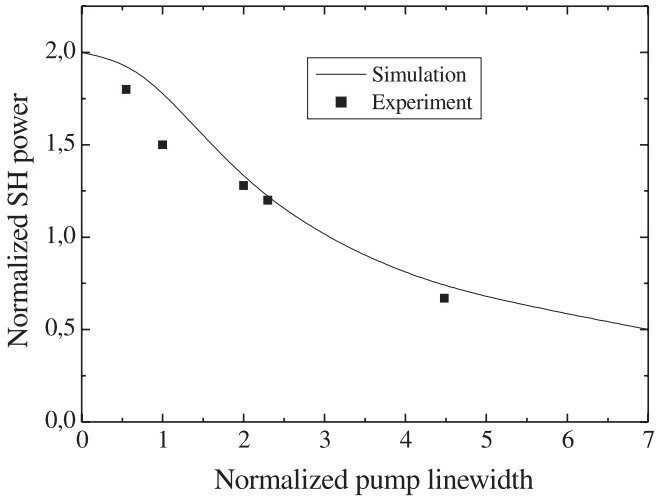

FIGURE 6 SH power, generated with a multi-mode pump as a function of pump line width. The output power is normalized by the corresponding single-mode case, and the line width is normalized by the acceptance bandwidth of the crystal. The *solid line* is obtained from [16]; the *squares* show the experimental data

one set of ω_b, Λ, and θ, but for any combination:

$$\eta_{\text{tot}} = 2\int_0^\infty \exp(-2(\omega_b'/\omega_b)^2) \times \frac{1}{2}(1+\cos(4\pi\omega_b'/l_b))\,\mathrm{d}\omega_b', \tag{11}$$

with $l_b = \Lambda/\sin(\theta)$ and the integration variable ω_b'. The numerical solution leads to the curve in Fig. 5. Here, the normalized conversion efficiency is plotted against the normalized beam radius ω_b/l_b. In Sect. 4, we will try to verify (10) and (11) and give quantitative experimental data.

3.3 *Optimizing the SHG efficiency*

From the above-mentioned effects, one can develop guidelines for optimizing the frequency conversion. The first thought, taking a crystal as long as possible and performing as many passes as possible with a wedge as small as possible, will soon see its practical limitations. To overcome the acceptance bandwidth problems, two main points should be taken into account. Most important, the fundamental laser should have a narrow line width or ideally oscillate in a single mode. Furthermore, an N-pass scheme through a short crystal should be performed rather than a single pass through a long crystal. This is because the efficiency increases with $N^2 l$ when the beam is re-imaged with the same spot size, while the acceptance bandwidth scales with $(Nl)^{-1}$ only. A single-pass scheme shows the same bandwidth behavior, but the efficiency scales only with Nl. These considerations are particularly important for the large-signal case, as shown in Fig. 3, where thermally induced perturbations limit the available acceptance bandwidth even further. For a more quantitative estimation, one can use the theory presented in [18] and determine the relation between the SHG efficiency and the ratio of the incident pump line width to the crystal acceptance bandwidth (see Fig. 6). Together with the above-presented equations, this leads to a solution that makes a balance between complexity and total SHG efficiency. In other words, a large number of passes through a very short crystal may lead to excellent SHG efficiency, but it may also exceed the acceptable amount of complexity (multiple mirrors with precise control needed).

4 Experimental results and discussion

4.1 *Fundamental laser sources*

For all the systematic investigations presented in this article, we used diode-pumped non-planar monolithic ring oscillators (NPROs). They are well-known sources of ultra-stable, continuous-wave single-frequency radiation with output powers exceeding 2 W [23]. Operation at 1064 nm has been reported as well as at 946, 1319, 1357, 1440, and 2020 nm (InnoLight GmbH). These lasers can be rapidly tuned via a piezoelectric element (1–2 MHz/V, 100-kHz modulation bandwidth) and also slowly by controlling the laser-crystal temperature ($\approx$ 3 GHz/K). Due to the monolithic design, the spectral line width is typically 1 kHz over a 100-ms time period. Although these properties make NPROs perfectly suited for our needs, we will also compare their performance as fundamental light sources with that of a regular multi-mode laser. It was a diode-pumped Nd : YAG laser with a linear flat–flat cavity and a line width of $\Delta\lambda = 0.30$ nm, centered at 1064 nm. The beam quality of all the lasers employed was close to diffraction limited and the polarization was linear. The maximum output power was 3.4 W for the NPRO and 8 W for the multi-mode laser.

In the first set of experiments, we used the NPROs to evaluate the effective nonlinear coefficient of the different PPKTPs in a simple single-pass scheme with confocal focusing.

4.2 *Evaluating d_{eff} of each crystal*

In a first set of experiments we studied single-pass SHG and sum-frequency generation (SFG) in PPKTP using NPROs at 946, 1064, and 1357 nm. By this we get data on the various samples, which could be used to understand the multi-pass experiments to come. The PPKTPs were flux-grown and

Sample	λ_F [nm]	Λ [μm]	L [cm]	η [$W^{-1}\,cm^{-1}$]	d_{eff} [$pm\,V^{-1}$]
1	946	6.09	0.84	1.06	9.8
2	1064	9.00	0.9	0.82	10.2
3	1064	9.00	2	1.05	11.8
4	1064	9.00	3	0.95	11.5
5	1064 + 1357	12.77	0.9	0.53	9.9
6	1357	17.71	0.65	0.34	9.4

TABLE 2 Data on the PPKTP samples evaluated in the experiments

poled according to the process described in [6]. It should be noted that all crystals had a uniform grating structure. The influence of non-uniform grating structures on the nonlinear process is presented in [12].

In the first experiment we used an 8.4-mm-long sample with a period of 6.09 μm for first-order QPM SHG of 946-nm radiation. The continuous-wave NPRO had an output power of 1.57 W at 946 nm. A blue power of 22 mW was obtained in single-pass frequency doubling, which corresponds to a normalized efficiency of 1.06 % $W^{-1}\,cm^{-1}$ and $d_{eff} = 9.8$ pm/V. In the second experiment, we used a 9-mm-long sample with a period of 9.00 μm. Focusing the output power of 1 W at 1064 nm from an NPRO confocally into this crystal resulted in a green SH power of 7.4 mW. This corresponded to a normalized efficiency of 0.82 % $W^{-1}\,cm^{-1}$ and $d_{eff} = 10.2$ pm/V. The same experiment was repeated with 2-cm- and 3-cm-long crystals. The deduced effective nonlinearities were here $d_{eff} = 11.8$ and 11.5 pm/V, respectively. Frequency conversion into the red spectral region was done by doubling the output of a NPRO at 1357 nm. A fundamental power of 550 mW, focused into an uncoated 6.5-mm-long PPKTP with a period of 17.71 μm, resulted in a red power of 0.58 mW. Taking into account the Fresnel losses, this corresponds to a normalized efficiency of 0.34 % $W^{-1}\,cm^{-1}$ and $d_{eff} = 9.4$ pm/V. In [24], we generated 16.7 mW of orange light at 596 nm with a normalized efficiency of 0.53 % $W^{-1}\,cm^{-1}$ and $d_{eff} = 9.9$ pm/V by SFG between a NPRO at 1064 and 1357 nm. All these results are summarized in Table 2.

4.3 *Experimental acceptance bandwidths and conversion efficiencies for different SHG schemes*

After determining the potential of each crystal, we tried to increase the conversion efficiency by employing different schemes. This could be done for all the crystals, but we restrict the experiments to SHG at 1064 nm, since the schemes are wavelength independent. The only difference would be the conversion efficiency (the conversion efficiency depends quadratically on the frequency of the radiation, see (6)) and an increasing absorption coefficient at lower wavelengths.

To verify the theoretically predicted limitations of SHG in PPKTP (see Sect. 3.1), we evaluated the acceptance bandwidths of the three 1064-nm samples specified above in single-, double-, triple-, and quadruple-pass combinations experimentally (see Fig. 6). For the double and triple passes, we used a uni-directional beam path. This was impossible for the quadruple pass, since the width of our crystals was limited. Here, we performed first a double pass and then directed the beam back again. It was then necessary to use a Faraday isolator to prevent destabilizing effects due to back-coupling into the laser cavity. All the basic bandwidth investigations were done in the small-signal regime (100-mW pump power at 1064 nm) to avoid the thermal perturbations that occur due to green and IR absorption in PPKTP. In all schemes, we focused and refocused confocally according to [17].

By temperature tuning the PPKTP in the single-, double-, and quadruple-pass schemes, we obtained the FWHM temperature acceptance bandwidths. They scaled from $\Delta T = 6.02$ K for single-pass SHG with the 0.9-cm-long sample to $\Delta T = 0.43$ K for quadruple-pass SHG with the 3-cm-long sample. As can be seen in Table 3, where the results are collected, one can find a reasonably good agreement between experiments and calculations. Small deviations can be explained by the non-ideal temperature-control loop (it was not possible to perfectly isolate the PPKTP mount).

The wavelength acceptance bandwidths were determined by tuning the temperature of the NPRO (see Sect. 4.1). This was restricted to the schemes where the bandwidth was two times smaller than the tuning range of the NPRO ($\Delta\nu \approx 8$ GHz). This method turned out to be very accurate and a bandwidth as narrow as 0.027 nm was measured for the quadruple-pass SHG, in good agreement with the theoretical estimate of 0.022 nm.

Finally, the angular bandwidth was investigated. The PPKTP samples were rotated around their z axis and the FWHM angular acceptance bandwidth was determined for the single-pass scheme. This measurement was calibrated by studying reflection of a He–Ne laser beam on the input surface and measuring the angular deflection. The experimental results again show good agreement with the theoretical values (see

L [cm]	N	ΔT_{exp} [K]	ΔT_{theo} [K]	$\Delta\lambda_{exp}$ [nm]	$\Delta\lambda_{theo}$ [nm]	$\Delta\varphi_{exp}$ [deg]	$\Delta\varphi_{theo}$ [deg]	η_{exp} [% W^{-1}]	$\eta_{theo,ideal}$ [% W^{-1}]	η_{theo} [% W^{-1}]
0.9	1	6.02	6.60		0.30	4.1	3.3	0.74	0.74	0.74
	2	2.81	3.30		0.15			2.39	2.96	2.75
	4	1.06	1.65		0.075			7.19	11.84	9.54
2	1	2.39	2.97		0.13	2.6	2.3	2.10	2.10	2.10
	2	1.05	1.49		0.067			7.45	8.40	7.50
	4	0.49	0.74	0.033	0.034			21.53	33.60	25.44
3	1	1.79	1.98		0.090	1.7	1.9	2.86	2.86	2.86
	2	0.77	0.99	0.048	0.045			9.70	11.44	9.50
	4	0.43	0.49	0.027	0.022			27.31	45.76	26.26

TABLE 3 Experimental and theoretical bandwidths for samples 2, 3, and 4 in single-, double-, and quadruple-pass schemes, together with the measured small signal conversion efficiencies. For the ideal efficiency $\eta_{theo,ideal}$, we only multiplied with N. For the real case η_{theo}, we considered absorption and interference as well as pump depletion effects

Table 3). For example, the 3-cm-long sample gives $\Delta\varphi = 1.7°$ experimentally, compared to $\Delta\varphi = 1.9°$ obtained from (9).

4.4 *Experimental consequences of acceptance bandwidth limitations*

At first sight, the extremely narrow spectral line width of the NPRO gave no reason to assume a degradation of the conversion efficiency even in the scheme with the smallest acceptance bandwidth. If this is true, then the deviation between experiment and theory (see Table 3) must originate from other loss mechanisms. For example, a quadruple pass through the 2-cm-long PPKTP should theoretically give an enhancement of 16 times compared to the single-pass SHG (see Sect. 3.2), but experimentally it only gave a 10 times enhancement (see Table 3). One already predicted contribution for the degradation is the phase-front distortion at the output boundary of the PPKTP (see Sect. 3.2). In Sect. 4.5, this problem will be treated in detail. Other contributions are quickly found. First, there are coating losses at the input and output surfaces of the PPKTP sample and the mirrors. Furthermore, there are absorption losses in KTP, which are non-negligible. In [25], the absorption coefficients have been measured to be $\alpha \approx 0.025\,\mathrm{cm}^{-1}$ at 532 nm and $\alpha < 0.01\,\mathrm{cm}^{-1}$ at 1064 nm for radiation polarized along the z axis, but it is well known that there are significant variations between samples, particularly between those fabricated by different growth techniques. In our case we measured $\alpha \approx 0.041\,\mathrm{cm}^{-1}$ at 532 nm and $\alpha < 0.006\,\mathrm{cm}^{-1}$ at 1064 nm in a single-pass configuration. We have concluded that the absorption and the coating losses contributed to half of the degradation while the other half was caused by phase-front distortion (quantitative data on the losses due to phase-front distortion will be given in Sect. 4.5). In the case of the NPRO, the efficiency was not limited by the acceptance bandwidths.

In contrast, SHG with the multi-mode laser is dominated by acceptance bandwidth limitations. One can see here a clear relation between the ratio of the incident pump line width to the crystal acceptance, and the conversion efficiency. We verified the theory presented in [16] by frequency doubling the multi-mode Nd : YAG laser in several SHG schemes with different acceptance bandwidths. The experimental results fit the theory quite well, as shown in Fig. 7. The consequences of this effect are also seen when comparing temperature-tuning curves for a small and a large normalized pump line width (ratio between pump line width and wavelength acceptance bandwidth). The two curves in Fig. 8 were taken with

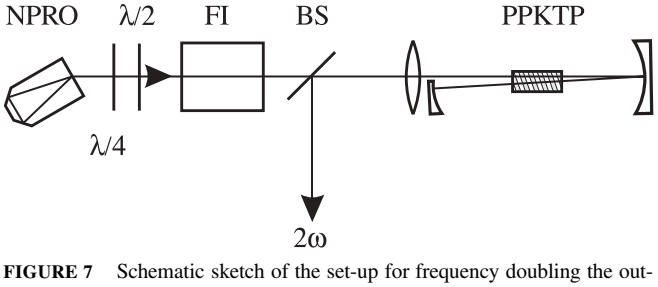

FIGURE 7 Schematic sketch of the set-up for frequency doubling the output of a NPRO in a quadruple-pass scheme through PPKTP. The wave plates are used to linearize the polarization of the fundamental beam, before propagating through the Faraday isolator FI and the beam splitter BS

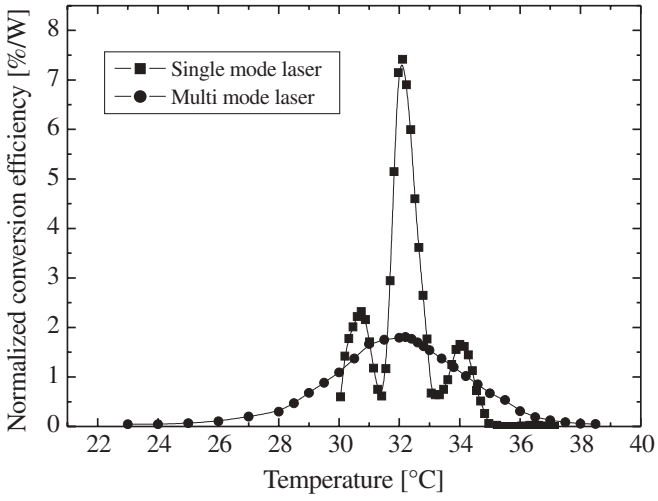

FIGURE 8 Experimental temperature-tuning curves under multi-mode and single-mode pumping in the large-signal regime. The generated SH power is 0.8 W

a double-pass scheme through sample 3 (2-cm long). We generated the same SH power (800 mW) when using 7.3 W of multi-mode pump power in the first case and 3.4 W of single-frequency pump power in the second case. One can clearly see how a large normalized pump line width spreads out the temperature tuning. From this, it becomes obvious that the first thing to consider when designing for a high SH conversion efficiency in a multi-pass experiment would be the normalized pump line width.

We performed an additional experiment to visualize this further. We compared a triple-pass SHG through a 5-mm-long PPKTP with a double pass through a 2-cm-long PPKTP using a power of 8 W from the longitudinal multi-mode laser. In the first experiment we obtained a SH output of 1.61 W and in the latter 1.23 W, which is more than 23% lower. This is in sharp contrast to what would have been obtained using a single-mode laser where the latter case would have given almost twice as high a SH output power as the first. A summary of the SH output powers and conversion efficiencies for the different schemes is given in Table 5.

4.5 *Experimental consequence of wedge angle* θ

In this section we investigate the problems that occur due to the angle formed between the grating and the crystal boundary. It might be possible to polish the crystal face in such a way that this angle becomes zero, but it is in practice very difficult to control the thickness of the last domain and hence the phase shift between the fundamental and the SH wave for the second pass through the crystal. However, with the dispersion in air, this could be corrected on the way back and forth between the crystal and the reflecting mirror. Between light at 1064 and 532 nm, the phase shift is $0.29\,\pi/\mathrm{cm}$ [26] in air at room temperature for standard pressure. Mirrors with different radii of curvature could be used to support the needed phase correction. Pearl et al. presented another solution. A thin glass plate was inserted into the cavity and the dispersive path length was controlled by tilting it [26]. Although we proved both methods to work well, they are not

Sample	θ_{S1} [mrad]	θ_{S2} [mrad]	ω_b [μm]	$\theta_{95\%}$ (10) [mrad]	$\theta_{95\%}$ (11) [mrad]
2	12.2	11.8	30.6	29.0	21.2
3	9.0	8.6	43.2	20.9	15.0
4	15.0	15.0	53.0	17.0	12.2

TABLE 4 Wedge angles for both sides of samples 2 to 4, as well as the beam radius at the crystal boundary ω_b and the angle where the conversion efficiency should drop to 95% of the maximum value (calculated with (10) and (11))

needed in our experiments, since the PPKTPs are cut with an arbitrary wedge angle and we corrected the phase shift by translating the PPKTP in the y direction [21].

To verify (11), we first needed to determine the wedge angles θ. This was done by performing a double pass through the crystals while observing the SH-power modulation that occurs when translating the back-reflected beam in the y direction over the whole crystal aperture. From the number of maxima and minima it was possible to deduce the wedge angles. They are given in Table 4 for both sides of samples 2 to 4, together with the fundamental beam radii ω_b at the crystal input and exit surfaces and the maximum allowable wedge angle, obtained from (10). To investigate the influence of ω_b on the conversion efficiency, we translated the PPKTP in the x direction, instead of changing the focusing strength. Then we compared the ratio of single-pass and double-pass SH power. Moving the crystal closer to the reflecting mirror results in a larger ω_b and hence a larger phase-mismatched part of the beam. This is shown in Fig. 5, where the above-mentioned ratio is plotted against ω_b for PPKTP sample 3. A comparison with the theoretical predictions is also made. Even if (11) describes the experimental results better than (10), the discrepancy is still quite large. One reason for this behavior may be that we also changed the waist location when translating the PPKTP. Therefore, optimum refocusing is no longer guaranteed. Another reason lies in the plane-wave nature of (11). It is an adequate but not perfect simplification in our case. For getting more precise theoretical predictions, one would need to consider the Gaussian nature of the beams. However, this would lead to complicated calculations and was hence intentionally left out of this work.

4.6 *Experimental consequences of SH absorption induced temperature perturbation*

As mentioned previously, PPKTP has substantial absorption in the green, as well as in the IR spectral region. Together with rather low heat conductivity, this leads to a noticeable temperature perturbation at modest signal power. Temperature, wavelength, and angular acceptance bandwidths are then inevitably affected.

Indeed, the phase-matching curves differ substantially from the small-signal one when scaling the NPRO output power up to 1.34 W (see Figs. 9 and 10). At higher power

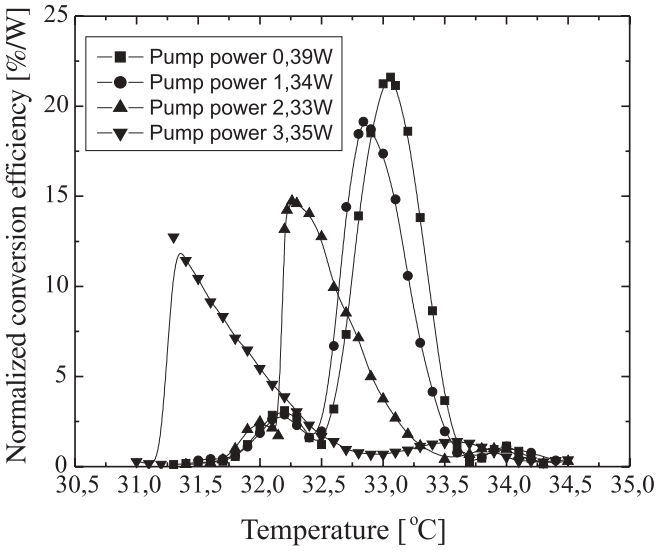

FIGURE 9 Experimental temperature-tuning curves for a quadruple pass through a 3-cm-long PPKTP with a single-mode laser as pump source. The *line* with *squares* is for the small-signal case; the *other lines* are for 1.34, 2.33, and 3.35 W, respectively

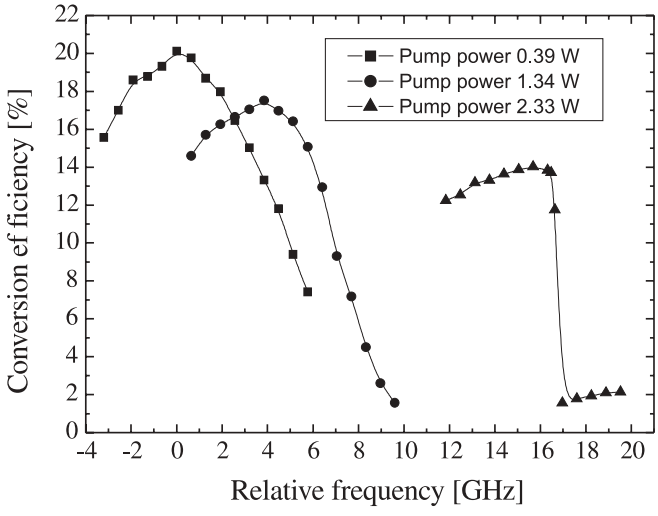

FIGURE 10 Experimental wavelength-tuning curves for a quadruple pass through a 2-cm-long PPKTP with a single-mode laser as pump source. The *line* with *squares* is for the small-signal case; the *other lines* are for 1.34 and 2.33 W, respectively

Scheme	Multi-mode SH power [W]	$\eta_{exp,multi\text{-}mode}$ [% W^{-1}]	Single-frequency SH power [W]	$\eta_{exp,single\ mode}$ [% W^{-1}]
Single pass 0.5 cm	0.53	0.83		
Double pass 0.5 cm	1.10	1.72		
Triple pass 0.5 cm	1.61	2.52		
Single pass 2 cm	1.00	1.56		
Double pass 2 cm	1.23	1.92	0.83	7.18
Quadruple pass 2 cm			1.42	12.28
Quadruple pass 3 cm			1.56	13.49

TABLE 5 Highest experimental SH powers and conversion efficiencies achieved in the different schemes with 8 W of multi-mode and 3.4 W of single-frequency pump power

(from around 2.3 W), we could even observe hysteresis effects for the temperature phase-matching curve, which means that the temperature-tuning curve differed slightly depending on if the scan was done by increasing or decreasing the temperature. For example, with a pump power of 3.4 W and a quadruple pass through the 3-cm sample, the position of the steep lower flank of the temperature tuning was 0.5 °C higher when tuning from lower to higher temperature, compared to the one obtained when tuning in the opposite direction.

The effect on the normalized conversion efficiency is of course strong but weaker for the NPRO, since it has such a small normalized pump line width. With this laser running at maximum power (3.4 W), the conversion efficiency decreased from 27.3 % W^{-1} to 13.4 % W^{-1} for the quadruple pass through the 3-cm-long crystal and from 21.3 % W^{-1} to 12.7 % W^{-1} for the 2-cm-long crystal. We have plotted the degradation of the normalized conversion efficiency for the different schemes in Fig. 11. Although it seems that the normalized efficiency for the quadruple-pass schemes flattens out at higher pump powers, it should be clear that the hysteresis effect decreases the practicality, meaning that temperature control for stable output power gets more and more difficult. However, we did not exceed this limit with the powers employed in our experiments. To conclude the investigation, we measured the SH power slope efficiencies. They are shown in Fig. 12 for the three different schemes. In all cases, the output power grows continuously without any visible turn over.

It should be mentioned that these results were only possible to be obtained with careful mounting of the PPKTP crystals. We glued the crystals into temperature-controlled copper mounts consisting of a base plate and a top cover to minimize thermal fluctuations and to guarantee optimum thermal contact.

When the multi-mode laser was frequency doubled a completely different behavior was observed. The wide line width reduces the normalized conversion efficiency much more than it did for the NPRO. In the experiments we found it not useful to employ a scheme with a larger normalized line width than 4, which was equivalent to a double pass through the

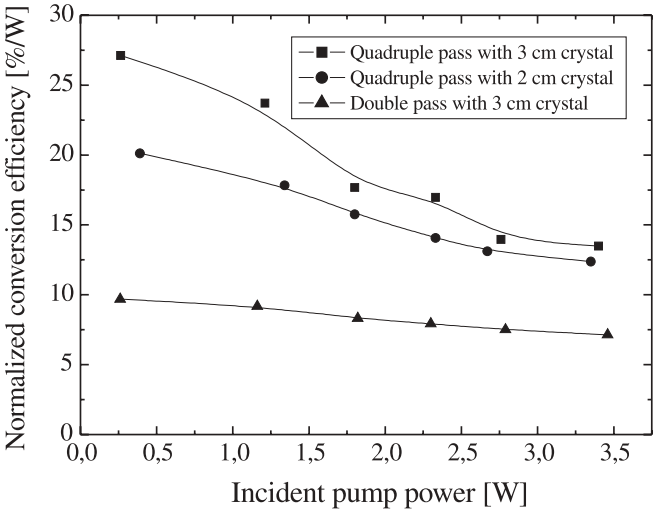

FIGURE 11 Degradation of the normalized conversion efficiency vs. single-mode pump power for different schemes

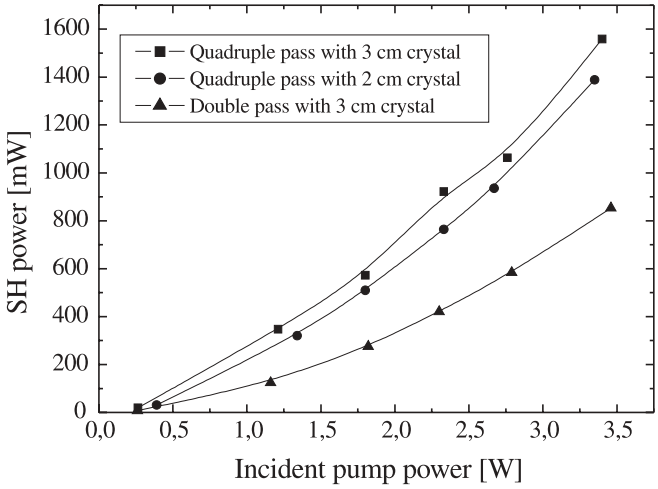

FIGURE 12 SH output power slope efficiency for single-mode pump in different schemes

2-cm-long PPKTP. In this case, the normalized conversion efficiency drops by 60% in the large-signal regime using the multi-mode laser (8 W at 1064 nm) but only by 22% with the NPRO (3.4 W at 1064 nm). It can be seen in the low-signal regime that multiple passes through a shorter crystal is advantageous. We achieve 4.71 % W^{-1} for a double pass through the 2-cm crystal and 4.92 % W^{-1} for a triple pass through the 0.5-cm crystal. The difference is even bigger in the large-signal regime. We obtain a maximum conversion efficiency of 2.52 % W^{-1} for a triple pass through the 0.5-cm-long PPKTP and 1.92 % W^{-1} for a double pass through the 2-cm crystal (see Table 5). Although the green power of 1.61 W is close to the one obtained with the NPRO, the needed pump power of 8 W is much higher (as expected from Fig. 7).

5 Conclusion

This study highlights the potential of SHG with PP media. We have investigated possible optimizations in SH output power generation using multiple passes through PP crystals of fixed length, both theoretically and experimentally. By using the guidelines, summarized in Sect. 3.3, and confirmed by the experimental results in Sect. 4, one can find an optimum scheme for any laser with defined line width and power. To the best of our knowledge we have hereby been able to generate the highest conversion efficiency ever reported for a non-resonant SHG scheme using a continuous-wave laser in a bulk nonlinear crystal. Power scaling to close to 2 W of SH power at 532 nm was demonstrated.

REFERENCES

1 M. Yamada, N. Nada, M. Saitoh, K. Watanabe: Appl. Phys. Lett. **62**, 435 (1993)
2 K. Mizzuchi, K. Yamamoto, M. Kato: Appl. Phys. Lett. **70**, 1201 (1997)
3 J.-P. Meyn, M.E. Klein, D. Woll, R. Wallenstein, D. Rytz: Opt. Lett. **24**, 1154 (1999)
4 M. Oron, M. Katz, D. Eger, G. Rosenman, A. Skliar: Electron. Lett. **33**, 807 (1997)
5 H. Karlsson, F. Laurell, P. Henriksson, G. Arvidsson: Electron. Lett. **32**, 556 (1996)
6 H. Karlsson, F. Laurell: Appl. Phys. Lett. **71**, 3474 (1997)
7 H. Karlsson, F. Laurell, L.K. Cheng: Appl. Phys. Lett. **74**, 1519 (1999)

8 G.D. Miller, R.G. Batchko, W.M. Tulloch, D.R. Weise, M.M. Fejer, R.L. Byer: Opt. Lett. **22**, 1834 (1997)
9 Q. Chen, W.P. Risk: Electron. Lett. **30**, 1516 (1994)
10 I. Juwiler, A. Arie, A. Skiliar, G. Rosenman: Opt. Lett. **24**, 1236 (1999)
11 F. Laurell: Opt. Mater. **11**, 235 (1999)
12 M.M. Fejer, G.A. Magel, D.H. Jundt, R.L. Byer: IEEE J. Quantum Electron. **QE-28**, 2631 (1992)
13 W.P. Risk: Proc. SPIE **2700**, 78 (1996)
14 J.A. Armstrong, N. Blombergen, J. Ducuing, P.S. Pershan: Phys. Rev. **127**, 1918 (1962)
15 S. Wang, V. Pasiskevicius, F. Laurell, H. Karlsson: Opt. Lett. **23**, 1883 (1998)
16 S. Helmfrid, G. Arvidsson, J. Webjörn: J. Opt. Soc. Am. B **10**, 222 (1992)
17 G.D. Boyd, D.A. Kleinman: J. Appl. Phys. **39**, 3597 (1968)
18 S. Helmfrid, G. Arvidsson: J. Opt. Soc. Am. B **8**, 2326 (1991)
19 B. Boulanger, J.P. Fève, Y. Guillien: Opt. Lett. **25**, 484 (2000)
20 M.E. Innocenzi, H.T. Yura, C.L. Fincher, R.A. Fields: Appl. Phys. Lett. **56**, 1831 (1990)
21 G. Imeshev, M. Proctor, M.M. Fejer: Opt. Lett. **23**, 165 (1998)
22 G.T. Moore, K. Koch: J. Opt. Soc. Am. B **16**, 781 (1999)
23 I. Freitag, A. Tünnermann, H. Welling: Opt. Commun. **115**, 511 (1995)
24 S. Spiekermann, H. Karlsson, F. Laurell, I. Freitag: Electron. Lett. **36**, 543 (2000)
25 G. Hansson, H. Karlsson, S. Wang, F. Laurell: Appl. Opt. **39**, 5058 (2000)
26 S. Pearl, H. Lotem, Y. Shimony, S. Rosenwaks: J. Opt. Soc. Am. B **16**, 1705 (1999)